

Self-organized escape processes of linear chains in nonlinear potentials

Torsten Gross^{*1}, Dirk Hennig², and Lutz Schimansky-Geier¹

¹Department of Physics, Humboldt-University at Berlin,
Newtonstr. 15, D-12489 Berlin, Germany

²Department of Mathematics, University of Portsmouth,
Portsmouth, PO1 3HF, United Kingdom

May 10, 2013

Abstract

An enhancement of localized nonlinear modes in coupled systems gives rise to a novel type of escape process. We study a spatially one dimensional set-up consisting of a linearly coupled oscillator chain of N mass-points situated in a metastable nonlinear potential. The Hamilton-dynamics exhibits breather solutions as a result of modulational instability of the phonon states. These breathers localize energy by freezing other parts of the chain. Eventually this localised part of the chain grows in amplitude until it overcomes the critical elongation characterized by the transition state. Doing so, the breathers ignite an escape by pulling the remaining chain over the barrier. Even if the formation of singular breathers is insufficient for an escape, coalescence of moving breathers can result in the required concentration of energy. Compared to a chain system with linear damping and thermal fluctuations the breathers help the chain to overcome the barriers faster in the case of low damping. With larger damping, the decreasing life time of the breathers effectively inhibits the escape process.

1 Introduction

A chain of binary interacting units is a simple model for discussing the emergence of collective phenomena. Despite its simplicity, such setup appears frequently in various physical contexts such as for the description of mechanical and electrical systems, polymers, networks of superconducting elements, chemical reactions in connected discrete boxes, to name but a few [1, 2, 3, 4, 5, 6, 7].

In this study we use the linear chain and its cooperative dynamical phenomena as a paradigm of a multidimensional dynamical system. We aim to investigate escape processes of the chain out of a metastable state [8, 9] also known as the nucleation of a kink-antikink pair [10, 11, 12, 13, 14, 15, 16] in biased

*tgross@physik.hu-berlin.de

sinusoidal potentials. To this end we place a chain with linear springs being responsible for the interaction between the units in a nonlinear potential modelled by polynomial of 3rd degree. As will be seen, energy along the chain will become inhomogeneously distributed and parts of the chain with large elongations will collect energy from their neighbouring regions. Such localized modes of energy are known as breather-solutions and have been studied intensively in the past in various contexts including micro-mechanical cantilever arrays [1, 17, 18], arrays of coupled Josephson junctions [19, 20], coupled optical wave guides [21, 22], Bose-Einstein condensates in optical lattices [23], in coupled torsion pendula [24], electrical transmission lines [25, 26], and granular crystals [27].

We concentrate here on the escape process and elaborate how the localized breathers modify this process [29, 28]. For this purpose we consider first the pure deterministic set-up and study the properties of breathers arising on the chain whose units evolve in the nonlinear potential. In the second set-up we investigate thermally activated escape dynamics. The chain will be exposed to a thermal bath with temperature T . Consequently damping and noise is added to the deterministic dynamics accounting for coupled Langevin equations. Our main new findings concern the study of how a change of the friction coefficient modifies the escape process. While for stronger damping breather solutions do not play a significant role, in case of weak damping the escape times become even shorter compared to the deterministic case. Notably, the establishment of breathers along the chain helps the emergence of critical elongations from thermal fluctuations.

This work is structured as follows: In Sec. 2 we introduce the model of a linearly coupled chain situated in an external nonlinear potential describing a metastable situation. We study the critical transition state, i.e. the bottleneck configuration which the chain has to cross in order that a transition over the potential barrier takes place. In Sec. 3 we derive conditions for the modulational instability which determine the time scale for the growth of the breathers. We find two generic scenarios which govern the transition. With larger energy singular breathers achieve large elongations and can surpass the transition states alone. Differently, if the elongation of the breathers are too small, they undergo an erratic motion. On collision, breathers tend to merge. Thereby they cumulatively localize energy which can eventually cause the barrier crossing. In Sec. 4 we study the thermally activated escape of the interacting chain in the metastable potential landscape. Finally, we summarize our findings.

2 The one-dimensional chain model

We study an one-dimensional chain of N linearly coupled oscillators of mass m with elongations $q_n(t), n = 1, \dots, N$. The chain is positioned in a cubic external potential. Every mass point experiences a nonlinear force caused by the potential

$$V(q_n) = \frac{m\omega_0^2}{2}q_n^2 - \frac{a}{3}q_n^3$$

and spring forces created from the neighbours with spring constant κ . Periodic boundary conditions are applied. Positions of particles perpendicular to the potential variation are kept constant [28], (for an alternative case see [31, 30]). First, we assume that there is no noise and no damping, hence yielding a canonic

situation with a Hamiltonian dynamics and corresponding momenta $p_n(t)$, $n = 1, \dots, N$ canonically conjugate to the positions $q_n(t)$. Consequently the total energy of the chain is conserved.

In order to obtain dimensionless quantities we rescale units and parameters, $\tilde{q}_n = a/(m\omega_0^2)q_n$, $\tilde{p}_n^2 = a^2/(m^4\omega_0^6)p_n^2$ and $\tilde{t}^2 = \omega_0^2 t^2$. As a result, we remain with dimensionless Hamiltonian with one remaining parameter only, the effective coupling strength $\tilde{\kappa} = \kappa/(m\omega_0^2)$. In what follows we omit the tildes.

The Hamiltonian of the considered chain reads:

$$\mathcal{H} = \sum_{n=0}^{N-1} \left[\frac{p_n^2}{2} + \frac{\kappa}{2} (q_n - q_{n+1})^2 + V(q_n) \right], \quad V(q_n) = \frac{q_n^2}{2} - \frac{q_n^3}{3}.$$

The resulting equations of motion become

$$\ddot{q}_n + q_n - q_n^2 - \kappa (q_{n+1} + q_{n-1} - 2q_n) = 0, \quad q_{N+1} = q_1. \quad (1)$$

In this paper we will consider for our numerical simulations chains comprising $N = 100$ units. A study of the dependence of the escape process on the number of oscillators can be found in [29].

For the study of an escape, we initially place the units of the chain close to the bottom of the external potential, that is nearby $q_{min} = 0$ and provide them with energy E . As will be seen, the chain eventually generates critical elongations surpassing the potentials local maximum. This initiates a transition of the chain into the unbounded regime $q_n > q_{max} = 1$, $n = 1, \dots, N$, which we refer to as an escape. For a single particle to overcome the potential barrier it needs to be supplied with an energy $\Delta E = V(1) - V(0) = 1/6$.

In the following we want to illustrate that the generation of these critical states is efficient even in cases where the chain energy E is small compared to $E \ll N \cdot \Delta E$. This low-energy setting is obtained through the following initial preparation of the system

$$q_i^{\text{IC}} = \Delta q_i + \Delta \quad p_i^{\text{IC}} = \Delta p_i,$$

where Δq_i and Δp_i are small random perturbations taken from a uniform distribution within the intervals

$$\Delta q_i \in [-\Delta q^{\text{IC}}, \Delta q^{\text{IC}}] \quad \text{and} \quad \Delta p_i \in [-\Delta p^{\text{IC}}, \Delta p^{\text{IC}}],$$

and the coordinate shift, $0 < \Delta < 1$, is chosen to increase the system energy to a desired value. This procedure results in a variety of perturbed flat initial states comprising a specific energy which we view as a statistical ensemble.

2.1 Transition states

For Hamiltonian systems the local minima of the energy surface (in phase space) are Lyapunov stable. That is, orbits in the vicinity of a local minimum never leave it as their associated energy is conserved. Therefore, orbits with an energy exceeding the energy associated with a neighbouring saddle point of first order are no longer bound to the basin. Thus the saddle point is referred to as transition state, as it separates bounded from unbounded orbits. Concerning our problem, the system's energy has to exceed the transition state energy

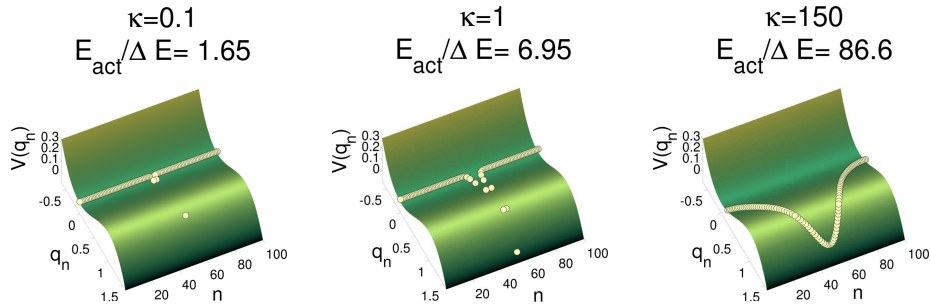


Figure 1: Transition state chain configurations for different values of κ . $N = 100$

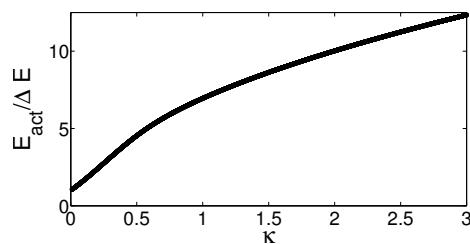


Figure 2: Activation energy (energy of transition state configurations), $N = 100$

to make escape events possible. To determine these transition states, we have to solve $\nabla U(q_1, q_2, \dots) = 0$, where U denotes the potential energy (thus the transition state is a fixed-point) and the solution must render all eigenvalues of the Hessian matrix of U positive, except for a single negative one. In general, this is a non-trivial task requiring sophisticated numerical methods. Here, we used the dimer method. It is a minimum-mode following method that solely makes use of gradients of the potential surface. It was first introduced in [32] and its computational effort scales favorably with the system size.

In the one-dimensional chain model the transition state configurations solve the stationary equation¹

$$q_n - q_n^2 - \kappa(q_{n+1} + q_{n-1} - 2q_n) = 0 \quad (2)$$

and fulfill the condition on the eigenvalues, λ^H , of the Hessian matrix H

$$H_{i,j} = \delta_{i,j}(2\kappa + 1 - 2q_i) - \kappa(\delta_{i,j+1} + \delta_{i,j-1}).$$

In the case of a vanishing coupling strength the oscillators and thus the equations of motion (1) are no longer coupled. Consequently, the fixed points of the system consist of all the configurations where each oscillator is placed either on the maximum of the potential barrier or the potential valley, $q_n^* = \{0, 1\}$. In this case also the Hessian matrix, H , becomes diagonal and we can directly read off its eigenvalues, $\lambda_n^H = 1 - 2q_n$. Demanding all eigenvalues to be negative except for one positive the transition states are found to be all the configurations where all oscillators are positioned in the potential valley except

¹An alternative approach for the one-dimensional chain model is presented in [28]. It casts the stationary equation into a two-dimensional map and links the localized lattice solutions to its homoclinic orbits.

for one that is placed on the potential barrier. The according energy reads $E_{\text{act}}(\kappa = 0) = \Delta E = 1/6$.

In contrast, a very large coupling strength corresponds to a situation where the chain effectively becomes a single oscillator so that the transition state refers to a chain configuration where all oscillators are placed on the maximum of the potential. This can be shown by taking the limit $\kappa \rightarrow \infty$ in Eq. (2). If we want q_n^* to take on values within a bounded regime we must have $q_{n+1}^* + q_{n-1}^* - 2q_n^* = 0$ in order to satisfy Eq. (2) in this limit. In the case of periodic boundary conditions this becomes equivalent to $q_n^* = q^*$ so that Eq. (2) becomes $q^*(1 - q^*) = 0$. Which of its two roots corresponds to the transition state becomes clear from the linear stability analysis of Eq. (1) for this effective one oscillator problem

$$\ddot{q} = -q + q^2 \approx -q^* + q^{*2} + (-1 + 2q^*)q = (-1 + 2q^*)q.$$

Only the case $q_n = q^* = 1$ is associated with the inherent instability of a transition state. Accordingly, the transition state energy is found to be $E_{\text{act}}(\kappa \rightarrow \infty) = N \Delta E = N/6$.

The intermediate parameter regime has been evaluated using the dimer method and the results are represented in Fig. 1 and Fig. 2. The maximal amplitude of the hair pin-like transition state configuration grows with increasing κ until it reaches a critical elongation from which on it decreases until the entire chain approaches the maximum of the potential barrier as described above.

3 The formation of breathers

3.1 Modulational instability of a chain in a nonlinear potential

The energy that is initially homogeneously distributed along the entire chain quickly concentrates into local excitations of single oscillators. This process is governed by the formation of regularly shaped wave patterns, so-called breathers which are spatially localized and time-periodically varying solutions. Their emergence is due to a modulation instability the mechanism of which applied to our situation is described later on. We follow [33] and [34] in this paragraph.

As an approximation for small oscillation amplitudes we can neglect the nonlinear term in Eq. 1. The resulting equation in linear approximation exhibits phonon solutions with frequency ω and wave number $k = 2\pi k_0/N$ (with $k_0 \in \mathbb{Z}$ and $-N/2 \leq k_0 \leq N/2$) related by the dispersion relation

$$\omega^2 = 1 + 4\kappa \sin^2\left(\frac{k}{2}\right)$$

We make an Ansatz that only takes into account the first harmonics (rotating wave approximation)

$$q_i = F_{1,i}(t) e^{-it} + F_{0,i}(t) + F_{2,i}(t) e^{-2it} + c.c.$$

The amplitudes of the harmonics are expected to be of a lower order of magnitude ($|F_{0,i}| \ll |F_{1,i}|$, $|F_{2,i}| \ll |F_{1,i}|$). Furthermore, we assume our envelope functions to vary slowly ($|\dot{F}_{m,i}| \ll |F_{m,i}|$) as well as the phonon band to be small

($1 > 4\kappa$). Within the limits of these assumptions we obtain a discrete nonlinear Schrödinger equation (DNLS) for the amplitudes of the first harmonic.

$$2i\dot{F}_{1,i} = \kappa((F_{1,i-1} + F_{1,i+1}) + 2F_{1,i}) - \frac{10}{3} |F_{1,i}|^2 F_{1,i} \quad (3)$$

We want to study the stability of this equation's plane wave solutions in the presence of small perturbations $|\delta B_i(t)| \ll 1$ and $|\delta \Psi_i(t)| \ll 1$, leading to a new Ansatz for the envelope function

$$F_{1,n}^{pert.} = (A + \delta B_n(t)) e^{i((kn - \Delta\omega t) + \delta \Psi_n(t))}. \quad (4)$$

The perturbations are sufficiently small so that we can expand the envelope function up to the first order in δ and neglect all terms of higher order. Using the Ansatz (4) in Eq. (3) leads to a complex differential equation for the perturbation functions $B(t)$ and $\Psi(t)$. The real and imaginary part of this equation are independent. Hence, collecting all terms of first order in δ results in two linear relations.

$$\begin{aligned} -A\dot{\Psi}_i &= -\frac{\kappa}{2} \{A \sin k (\Psi_{i-1} - \Psi_{i+1}) + \cos k (B_{i+1} + B_{i-1})\} - \frac{10}{3} A^2 B_i \\ 2\dot{B}_i &= -\kappa \{A \cos k (\Psi_{i+1} + \Psi_{i-1} - 2\Psi_i) + \sin k (B_{i+1} - B_{i-1})\} \end{aligned}$$

Again, the solution to those coupled equations are plane waves

$$\Psi_n = \Psi^0 e^{i(Qn - \Omega t)} \quad B_n = B^0 e^{i(Qn - \Omega t)}$$

with the dispersion relation

$$(\Omega - \kappa \sin k \sin Q)^2 = \kappa \cos k \sin^2 \left(\frac{Q}{2} \right) \left(4\kappa \cos k \sin^2 \left(\frac{Q}{2} \right) - \frac{20}{3} A^2 \right) \quad (5)$$

which describes the stability of the Q -mode perturbation on the k -mode carrier wave. Q and k have a 2π periodicity and can therefore be chosen to be in the first Brillouin zone. Furthermore, we can restrict the range of k and Q : $k, Q \in \{0, \pi\}$, because negative values correspond to waves with the opposite direction of propagation.

The perturbations are stable for $\Omega \in \mathbb{R}$ which is the case when the right hand side of Eq. (5) is positive. Therefore, all carrier waves with $k \in \{\pi/2, \pi\}$ are stable with respect to all perturbation modes. For $k \in \{0, \pi/2\}$ perturbations will grow, provided that

$$\cos k \sin^2 \left(\frac{Q}{2} \right) \leq \frac{5A^2}{3\kappa}. \quad (6)$$

We can then find an according growth rate

$$\Gamma(Q) = |\text{Im}(\Omega)| = \sin \left(\frac{Q}{2} \right) \sqrt{\frac{20}{3} \kappa \cos k \left(A^2 - \frac{3}{5} \kappa \sin^2 \left(\frac{Q}{2} \right) \cos k \right)} \quad (7)$$

which, for the case that $A^2 \leq \frac{6}{5} \kappa \cos k$, has its maximum at

$$Q_{\max} = 2 \arcsin \sqrt{\frac{5A^2}{6\kappa \cos k}}. \quad (8)$$

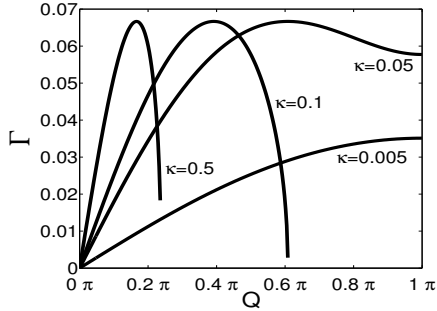


Figure 3: Growth rates of unstable Q -modes according to Eq. (7) from a $k=0$ carrier mode with $A=0.2$

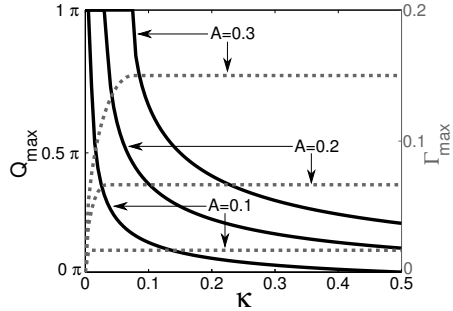


Figure 4: Fastest growing modes (solid line) - Eq. (8) - and their growth rates (dashed line), $k=0$.

Otherwise the maximum growth rate is found at $Q = \pi$. The corresponding growth rates become

$$\Gamma_{\max} = \begin{cases} \Gamma(Q_{\max}) = \frac{5}{3}A^2 & \text{if } A^2 \leq \frac{6}{5}\kappa \cos k \\ \Gamma(\pi) = \sqrt{\frac{20}{3}\kappa \cos k(A^2 - \frac{3}{5}\kappa \cos k)} < \Gamma(Q_{\max}) & \text{if } A^2 > \frac{6}{5}\kappa \cos k \end{cases} \quad (9)$$

We recall from Sect. 2 that our system is initially prepared in a slightly perturbed $k = 0$ mode. This is thus the only possible carrier wave mode as the amplitudes, A , of all other modes (which scale with the amplitude of the perturbation) are likely to be too small to generate growing modes – see inequality (6) – or the arising maximal growth rates are suppressed. Evaluating the growth rate of instabilities on the $k = 0$ carrier mode for different values of κ (Fig. 3), we find that the modulational instability becomes more mode selective with increasing κ . Hence, for large values of κ the only relevant unstable modes are near the fastest growing mode depicted in Fig. 4. In such a situation we expect the emergence of a regular wave pattern (an array of breathers) that efficiently localizes energy and thereby enhances the escape of the chain.

3.2 Optimal coupling

According to our findings in the previous section the appearing breather array becomes more regular with increasing κ . In particular its prominent mode number, and therefore the number of breathers, gets smaller, all of which results in an efficient energy localization. However, an increase in the coupling strength comes along with an increase in the activation energy – see Fig. 2 – which hinders a swift escape for a given system energy. Therefore, we can expect to find an intermediate κ that optimizes the escape rate.

We can analytically approximate the optimal κ by assuming that the entire system energy is evenly distributed among N_B non-interacting oscillators, where N_B is the number of breathers related to the prominent wave length, Q_{\max} , of the modulational instability. The ratio of such an oscillator's energy, E_B , to the activation energy can be regarded as a measure of escape efficiency. It is dependent on Q_{\max} which in turn depends on the $k = 0$ phonon amplitude A

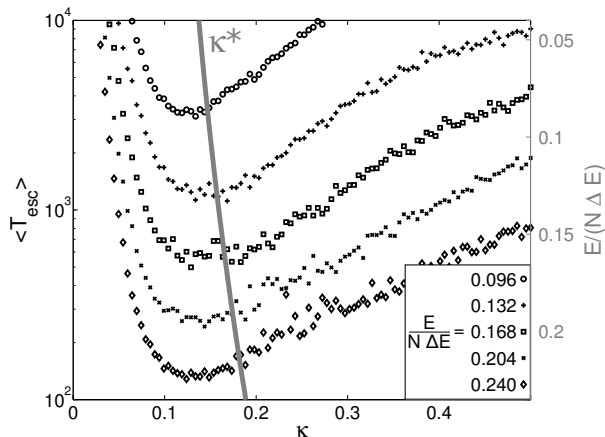


Figure 5: Average escape times (marker symbols) for 500 realizations with randomized initial conditions as described in Sec. 2. Parameters: $\Delta q^{\text{IC}} = 0.05$, $\Delta p^{\text{IC}} = 0.05$, $N = 100$. The solid grey line represents the analytical approximation for the optimal coupling strength – Eq. (10) – for energy values given by the right-hand axis.

which we relate to the system energy via $E(A) = NV(A)$. Thus we can write

$$\frac{E_B(\kappa)}{E_{\text{act}}} \propto \frac{1}{Q_{\text{max}}(E, \kappa) E_{\text{act}}(\kappa)}.$$

This escape efficiency takes on its maximum for the optimal coupling strength, κ^* , formally

$$\kappa^*(E) = \arg \max_{\kappa \in \mathbb{R}^+} \frac{1}{Q_{\text{max}}(E, \kappa) E_{\text{act}}(\kappa)}. \quad (10)$$

This approximation can now be compared to the numerical evaluation of average escape times in dependence of κ , see Fig. 5. Equation (1) has been integrated using a fourth order Runge-Kutta scheme. Numerical accuracy was obtained by ensuring the energy deviation to remain smaller than the order of 10^{-12} . The average escape times were determined from 500 realization of randomized initial conditions at a given energy according to Sec. 2 for each marker symbol. The escape time measures the time it takes from the initialization to the moment when all oscillators have surpassed the potential barrier. For all depicted values of κ at least 95 % of the chain realizations escaped in the maximal integration time of $5 \cdot 10^5$ time units.

Figure 5 clearly shows the predicted resonance behaviour and also reveals a fairly good accordance of the analytical approximation of the optimal κ with the simulation results. This seems to verify our initial assumption of a regular breather array that fully concentrates the energy into single oscillators. But this reasoning fails to explain the pronounced variation of the average escape times (ranging over several orders of magnitude) for different energies. Additionally, the equipartition of a low system energy will not allocate single breathers with an energy sufficient to trigger an escape event. E.g. for $\kappa = 0.15$ and $E/(N\Delta E) = 0.1$ we expect an array with ten or more breathers so that each one could only

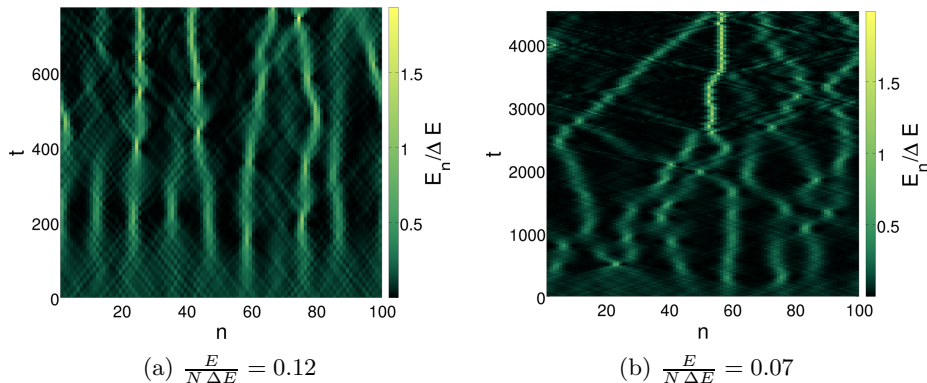


Figure 6: Temporal evolution of the energy distribution $E_n(t)$. The localization of energy from an initially homogeneous state causes in both cases an escape at the end of the depicted time frame. While the system energy in Fig. 6a is sufficiently high to let an individual breather of the early regular breather array surpass the potential barrier, the lower energy in Fig. 6b necessitates a merging of breathers to cause the critical chain elongation. Parameters: $\kappa = 0.15$, $\Delta q^{\text{IC}} = 0.05$, $\Delta p^{\text{IC}} = 0.05$, $N = 100$

hold an energy $E/N_B < \Delta E$. Nevertheless, an escape takes place, eventually. This implies a further concentration of energy beyond the initial creation of the breather array. In order to study this process, we look at the snapshots of the energy distribution

$$E_n = \frac{p_n^2}{2} + V(q_n) + \frac{\kappa}{4} \{(q_n - q_{n+1})^2 + (q_{n-1} - q_n)^2\},$$

In Fig. 6 E_n has been tracked in time (upwards) for two exemplary cases. Energy is localized in both cases starting from an initially homogeneous state. In Fig. 6a we see the appearance of a regular breather pattern. Every breather concentrates enough energy to certain oscillators in order to trigger an escape. In contrast, the lower system energy in Fig. 6b does not allow for a direct escape of the initial breathers. Instead, breathers start an erratic movement. After an inelastic interaction they merge and can thereby eventually result in a configuration exceeding the critical chain elongation, see also [35]. However, this secondary process is slow compared to the (direct) breather formation which explains the different orders of magnitude of the escape times scale in Fig. 5.

4 Thermally activated escape supported by breathers

In the previous sections we have been concerned with the deterministic chain dynamics leading to an escape event. In this section we study how a thermal bath with temperature T will modify the transition over the barrier. For this purpose we consider the associated Langevin equation,

$$\ddot{q}_n + q_n - q_n^2 - \kappa(q_{n+1} + q_{n-1} - 2q_n) + \gamma\dot{q}_n + \xi_n(t) = 0, \quad (11)$$

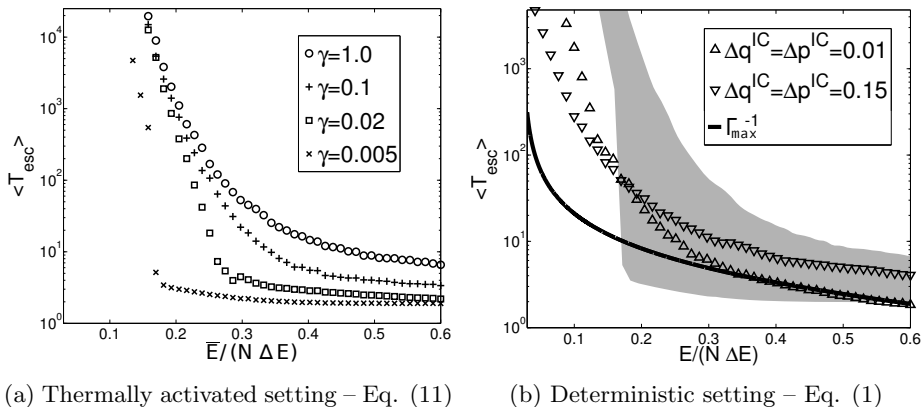


Figure 7: Average escape times in the thermally activated case for different values of the friction constant and their comparison to the deterministic setting for 500 realizations each. The grey area in Fig. 7b sketches the average escape times for the thermally activated case for $0.005 < \gamma < 1.0$ as shown in Fig. 7a where as the symbols shows results from the deterministic set-up with initial conditions given in the inset. Parameters: $\kappa = 0.15, N = 100$

with the friction parameter γ and a Gaussian white noise term $\xi_n(t)$. In order to be able to compare the deterministic situation to the thermally activated setting, the associated conserved energy E in the Hamiltonian case and the average energy \bar{E} transferred from the bath need to be equal. The latter is governed by the correlation function of the noisy force $\xi(t)$. Its permanent variation yields source of energy for the chain which is balanced by the dissipative friction forces.

The transferred energy is defined if the autocorrelations functions of the noise sources scale as

$$\langle \xi_n(t) \xi_{n'}(t') \rangle = 2\gamma \bar{E}/N \delta_{n,n'} \delta(t-t'). \quad (12)$$

This relation, known as fluctuation dissipation theorem, implies that the mean energy of all particles is given by \bar{E} . If expressed by the bath temperature, every particle gets in average $k_B T$, *i.e.* $\bar{E} = N k_B T$ with k_B being the Boltzmann constant.

In numerical simulations of the Langevin equation with fulfilled relation (12), we have assured that the full average energy converges to \bar{E} also for the transient state of the transition. Initially after the chain has relaxed to a stationary situation around the metastable minimum of the potential $V(q_{min})$, the oscillators obey the canonic distribution in phase space near to this minimum.

We measure average escape times for the system described by Eq. (11). The latter is numerically integrated using an Euler scheme, again with a maximal integration time of $5 \cdot 10^5$ time units. The system is initialized with all oscillators set to the minimum of the potential and zero momenta. We then let the system thermalize until its energy reaches \bar{E} for the first time. The time from this moment until all oscillators have surpassed the potential's maximum counts as the escape time.

We study the system for the optimal coupling constant, $\kappa = 0.15$, as described in Sec. 3.2. Figure 7a shows the average escape times of 500 realiza-

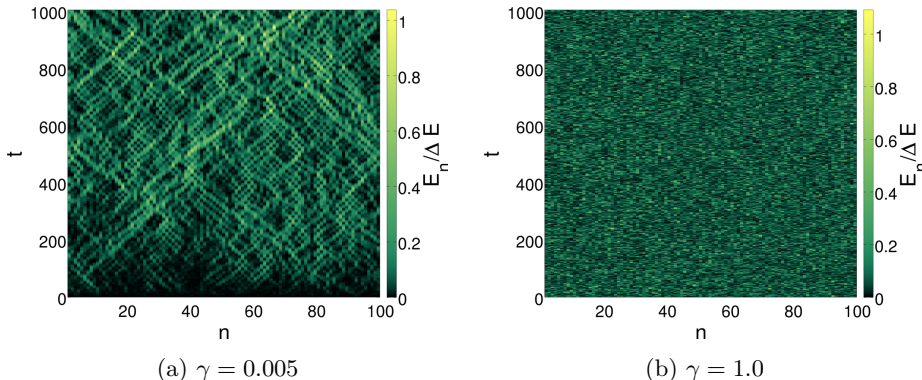


Figure 8: Temporal evolution of the energy distribution $E_n(t)$ in the thermally activated case. A smaller friction constant leads to a higher degree of energy localization. Parameters: $\overline{E}/(N \Delta E) = 0.15$, $\kappa = 0.15$.

tions for different values of the friction constant in dependence of \overline{E} . Figure 7b compares these times (depicted as the grey surface) to the according average escape times of the deterministic system. It additionally shows the characteristic time constant for the formation of breathers, Γ_{\max}^{-1} , taken from Eq. (9), where again we relate the $k = 0$ phonon amplitude, A , to the system energy via $E(A) = NV(A)$.

Especially for smaller energies the deterministic escape is considerably faster than the thermally activated one. Notably for $E/(N \Delta E) < 0.1$ and quite contrary to the deterministic setting, escape events are practically absent during our simulations time in the thermal case. For larger energy values this picture can change to a higher efficiency of the thermal escape process when damping is weak. Also two deterministic settings with different magnitudes of the random initial perturbations have a converse behaviour for low and high energies.

How can this result be explained by observations of the chain dynamics? For small values of γ the system approaches the deterministic setting. This entails an observable tendency towards a more localized energy distribution as seen in comparing Fig. 8a and Fig. 8b. The relaxation time of the chain scales with the inverse of the damping constant. Correspondingly, the life times of local excitations grow with decreasing γ . The outcome is a more heterogeneous energetic structure where thermal fluctuations are more likely to cause critical chain elongations. This explains the faster escape comparing small with large damping constants. But even in the case of very small γ the relaxation time is still much shorter than the time needed for the coalescence of multiple breathers (which is of the order of several hundred time units, see Fig. 6b). Therefore, the long term cumulative concentration of energy, as described in 3.2, is generally inhibited in the thermal case. This explains the virtual impossibility of a thermal escape for small energies.

In the opposite case of higher energies the deterministic escape is mostly proceeded by initial breathers. The formation time of the initial breather array can be estimated by the inverse of the maximal growth rate, Γ_{\max} from Eq. 9. Figure 7b shows the expected convergence of Γ_{\max}^{-1} to the deterministic escape times for large energies. We recall from Sec. 3 that Γ_{\max} was determined starting

with a linear expansion in the perturbations. We believe that this explains the better match in the case of smaller initial perturbations. The divergence of Γ_{\max}^{-1} with the average escape times for small energies again gives evidence to the fact that the initial breather array does not induce an escape and other mechanisms are needed.

In the thermally activated case the large energy setting holds two characteristic scenarios. The mobility of the breathers becomes amplified if noise acts. If the breathers possess longer life times, *i.e.* for smaller damping, a few (usually not more than two) breathers can temporarily merge and thus approach a critical chain elongation. Starting with a heterogeneous energy structure after thermalization, this then leads to smaller escape times compared to the deterministic setting that first has to re-allocate energy from an initially homogeneous state. Oppositely for stronger damping, the life times of breather is too short and the energy distribution is mostly homogeneous (see Fig. 8b). The escapes then relies entirely on rare, large enough spontaneous fluctuation of the noise term and the average escape times generally become comparatively large.

Finally, we want to examine the converse behaviour for different magnitudes of the initial perturbations in the deterministic case. As the initial conditions for smaller perturbations are closer to the $k = 0$ phonon mode the initial breather array emerges more quickly so that the escape times are smaller when the energy is high enough for initial breathers to ignite the escape. Contrarily, stronger perturbations lead to a higher breather mobility which accelerates the breather coalescence so that the escape times become smaller when low energy necessitates coalescence.

5 Summary

We have studied various examples of collective escape processes in many-particle systems. First we started with a noise-free escape in a chain of coupled oscillators evolving in a metastable potential. The second part of this work examined a thermally activated escape. To this end the original system has been augmented by a linear friction term and Gaussian thermal, white noise of vanishing mean satisfying the fluctuation dissipation theorem.

While a thermally activated escape becomes virtually impossible at low system energy, the deterministic system remains capable of efficiently crossing the potential barrier. In more detail, the deterministic dynamics of interacting chain units leads to the formation of breather solutions localizing energy such that the chain passes through a transition state and crosses the potential barrier. In particular at low system energy, the interaction between several formed breathers resulting in their coalescence eventually enables the chain to accumulate sufficient energy to overcome the potential barrier. Interestingly, in the thermally activated setting with a sufficiently weak damping, the breather formation and thermal fluctuation cooperate to localize energy which accomplishes effective barrier crossings.

We underline that the dynamics of interacting particles exhibiting collective behaviour such as breather formation and their interaction has a huge impact on the escape and activation dynamics in such many-body systems. Hence, our study intends to offer new perspectives on the understanding of such collective escape processes.

6 Acknowledgments

L. Schimansky-Geier thanks for support from IRTG 1640 of the Deutsche Forschungsgemeinschaft. The authors acknowledge previous co-authors for a successful cooperation.

Preprint of an article published in the book “First-Passage Phenomena and Their Applications”: pp. 554-570, May 2014; doi: 10.1142/9789814590297_0022 ©World Scientific Publishing Company.

References

- [1] M. Sato, B. E. Hubbard, and A. J. Sievers, *Rev. Mod. Phys.* **78**, 137–157 (2006).
- [2] S. Flach and C. R. Willis, *Phys. Rep.* **295** (5), 181–264 (1998).
- [3] T. Dauxois, M. Peyrard, and C. Willis, *Physica D* **57**, 267–282 (1992).
- [4] P. Reineker and R. G. Winkler, *Phys. Lett. A* **141**, 264–268 (1989).
- [5] M. Doi and H. See, *Introduction to Polymer Physics*, Oxford University Press (Oxford, 1995).
- [6] T. Erneux and G. Nicolis, *Physica D* **67**, 237 (1993).
- [7] V.A. Makarov, V.I. Nekorkin, V.B. Kazantsev, and M.G. Velarde, *Physica D* **100**, 330 (1997).
- [8] J.S. Langer, *Ann. Phys. (N.Y.)* **54**, 258 (1969).
- [9] P. Hänggi, P. Talkner and M. Borkovec, *Rev. Mod. Phys.* **62**, 251 (1990).
- [10] F. Marchesoni, P. Hänggi, and P. Sodano, In *Universalities in condensed matter*, eds. L. R. Jullien, L. Peliti and N. Boccara, *Springer Proc. in Physics* vol. 32, p. 88, Springer Verlag (1988).
- [11] P. Hänggi, F. Marchesoni and P. Riseborough, *Europhys. Lett.* **13**, 217–222 (1990).
- [12] M. Büttiker and T. Christen, *Phys. Rev. Lett.* **75**, 1895–1898 (1995).
- [13] T. Christen, *Europhys. Lett.* **31**, 181–186 (1995).
- [14] T. Christen, *Phys. Rev. E* **51**, 604–612 (2009).
- [15] K. Fedorov and A. Pankratov, *Phys. Rev. Lett.* **103**, 260601 (2009).
- [16] D.R. Gulevich, M.B. Gaifullin and F.V. Kusmartsev, *Eur. Phys. Journ. B* **85**, 24 (2012).
- [17] M. Sato, B.E. Hubbard, A.J. Sievers, B. Ilic, D.A. Czaplewski, and H.G. Craighead, *Phys. Rev. Lett.* **90** 044102 (2003).
- [18] M. Sato, B.E. Hubbard, L.Q. English, A.J. Sievers, B. Ilic, D.A. Czaplewski, and H.G. Craighead, *Chaos* **13** 702 (2003).

- [19] E. Trias, J. Mazo, and T. Orlando, *Phys. Rev. Lett.* **84** 741 (2000).
- [20] P. Binder, D. Abraimov, A.V. Ustinov, S. Flach, and Y. Zolotaryuk, *Phys. Rev. Lett.* **84** 745 (2000).
- [21] J.W. Fleischer, M. Segev, N.K. Efremidis, and D.N. Christodoulides, *Nature* **422** 147 (2003)
- [22] H.S. Eisenberg, Y. Silberberg, R. Morantotti, A.R. Boyd, and J.S. Atchinson, *Phys. Rev. Lett.* **81** 3383 (1998).
- [23] B. Eiermann, T. Anker, M. Albiez, M. Taglieber, P. Treutlein, K.P. Marzlin, and M.K. Oberthaler, *Phys. Rev. Lett.* **92** 23041 (2004).
- [24] J. Cuevas, L.Q. English, P.G. Kevredikis, and M. Anderson, *Phys. Rev. Lett.* **102**, 224101 (2009).
- [25] L.Q. English, M. Sato, and A.J. Sievers, *Phys. Rev. E* **77**, 066601 (2008).
- [26] P. Marquié, J.M. Bilbaut and M. Remoissenet, *Phys. Rev. E* **51**, 6127 (1995).
- [27] N. Boechler, G. Theocharis, S. Job, and P.G. Kevredikis, *Phys. Rev. Lett.* **104**, 244302 (2010).
- [28] D. Hennig, L. Schimansky-Geier and P. Hänggi, *Europhys. Lett.* **78** (2007) 20002
- [29] D. Hennig, S. Fugmann, L. Schimansky-Geier, and P. Hänggi, *Phys. Rev. E* **76**, 041110 (2007).
- [30] S. Martens, D. Hennig, S. Fugmann, and L. Schimansky-Geier, *Phys. Rev. E* **78**, 041121 (2008).
- [31] S. Fugmann, D. Hennig, L. Schimansky-Geier, and P. Hänggi, *Phys. Rev. E* **77**, 061135 (2007).
- [32] G. Henkelman and H. Jonsson, *Journ. of Chem. Phys.* **111**, 7010–7022 (1999).
- [33] Y. S. Kivshar and M. Peyrard, *Phys. Rev. A* **46**, 3198–3205 (1992).
- [34] I. Daumont, T. Dauxois, and M. Peyrard, *Nonlinearity* **10**, 617 (1997).
- [35] M. Peyrard, *Physica D* **119**, 184 – 199 (1998).